JMEPEG (2005) 14:582-590
DOI: 10.1361/105994905X64521

1059-9495/$19.00

Influence of the Stress, Strain, and Temperature on the Surface Roughness of an AISI 52100 Steel Due to an Orthogonal Cut

Patricia Muñoz-Escalona, Shreyes Melkote, and Kai Liu

(Submitted March 1, 2005; in revised form July 5, 2005)

In recent years, the finite element method (FEM) has become the main tool for simulating the metal cutting process because research based on trial and error is time consuming and requires high investment. Early studies were done by different investigators. In this research AISI 52100, hardened steel (62 HRC) was selected for an orthogonal machining process as well as metal cutting simulation using the software DEFORM-2D. This software is based on a forging process and has been adapted to an orthogonal machining process. The results of simulated cutting forces were compared with experimental cutting force data to validate the orthogonal cut simulation. Also, the surface roughness was measured, and the influence of the stress, strain, and temperature on the surface roughness was studied.

Keywords hard, orthogonal, polycrystalline cubic boron nitride (PCBN), process, turning

1. Introduction

Since 1930, several studies have been made in the area of cutting processes. The studies of chip formation were the main goal of the research since, from these studies, they could know the cutting forces, stresses, and temperatures involved in the process. Various methods were proposed, several of them based on the fundamentals of mechanical cutting processes and the others based on experimental expressions. The first person to model orthogonal metal cutting was Merchant (Ref 1), who introduced the concept of the shear angle (his results were very good for polymeric materials but not for metals). Lee and Schaffer subsequently proposed an analytical model using slip-line theory (Ref 2). Tay et al. (Ref 3) obtained temperature distributions for cases of orthogonal machining with continuous chip formation by solving the steady two-dimensional energy equation using the finite element method (FEM).

Hasting (Ref 4) described an approximate machining theory in which the temperature, strain rate, and workpiece properties were taken in account. The theory was applied to two plain carbon steels at different cutting conditions by using flow stress data obtained from high-speed compression tests.

Lee (Ref 5) conducted orthogonal machining experiments in 6061-T6 aluminum, 4340 steel and Ti-6Al-4V titanium to measure strain distribution in deformed chips using a grid analysis technique. Strenkowski and Carrol (Ref 6) described FEM on orthogonal metal cutting, introducing a new chip separation criterion based on the effective plastic strain in the workpiece. Several cutting parameters that are often neglected in simplified metal cutting models are included, such as elastic-plastic properties of workpiece and tool, friction along the tool rake face, and geometry of the cutting edge and workpiece. The model predicts chip geometry, residual stresses in the work piece and tool, and stresses and forces without any reliance on empirical metal cutting data. This paper also demonstrates that the use of a chip separation criterion based on effective plastic strain is essential in predicting chip geometry and residual stresses with FEM.

Childs and Maekawa (Ref 7) studied the development of an elastic-plastic and thermal finite element analysis of chip flow and stress, tool temperature, and wear in low alloy steels. The analysis needs further refinement, particularly in its tool force prediction capacity but has been helpful in tool temperature and wear prediction.

Other investigators have focused their experiments in orthogonal metal cutting using the FEM (Ref 8-14).

Patricia Muñoz-Escalona, Universidad Simón Bolívar, Departamento de Mecánica Caracas 1080, Venezuela; **Shreyes Melkote** and **Kai Liu,** Georgia Institute of Technology, Woodruff School of Mechanical Engineering, Atlanta, GA 30332-0560. Contact e-mail: pmunoz@usb.ve.

Nomenclature

$\varnothing_{ext}$	external diameter, mm
$\varnothing_{int}$	internal diameter, mm
f	feed rate, mm/rev
V	cutting speed, m/min
Fx	cutting force, N
Fy	thrust force, N
α	clearance angle, degrees
γ	rake angle, degrees
R	tool edge cutting radius, mm
R_t	maximum roughness height, μm
rms	root-mean-square average, μm
R_a	arithmetic mean value, μm
σ_c	shear stress

Table 1 Chemical composition of AISI 52100

%C	%Cr	%Fe	%Mn	%Si	%P	%S
0.98-1.10	1.40	97.05	0.35	0.25	<0.25	<0.25

Table 2 Physical and mechanical properties of AISI 52100

Property	Value
Density, kg/m^3	7827
Specific heat, J/kg °C	458
$25 < T < 204$	640
$204 < T < 426$	745
$426 < T < 537$	798
$T > 537$	
Thermal conductivity, W/m · K	46.6
Coefficient of thermal expansion, °C × 10^{-6}	12.6
Melting temperature, °C	1500
Yield strength, MPa	2427
Young's modulus, GPa	210
Poisson's ratio	0.277
Hardness(a), HRC	62

(a) To obtain 62 HRC, the steel was heat treated at 829 °C (1525 °F) for 15 h, quenched in oil, and tempered at 163 °C (325 °F) for 2 h.

Table 3 Physical and mechanical properties of PCBN tool

Property	Value
Density, kg/m^3	3420
Specific heat, J/kg °C	750
Thermal conductivity, W/m · K	100
Coefficient of thermal expansion, °C × 10^{-6}	4.90
Young's modulus, GPa	680
Poisson's ratio	0.22

2. Experimental Procedure

2.1 Workpiece Material and Characteristics

AISI 52100 carbon steel was used for the experiments with $\varnothing_{ext} = 41.275$ mm and $\varnothing_{int} = 27.05$ mm. Table 1 shows the chemical composition, and Table 2 shows the physical and mechanical properties of this steel.

2.2 Tool Material and Characteristics

Kennametal NG 3156l, Grade KD120, polycrystalline cubic boron nitride (PCBN) cutting tool, with a CBN content of approximately 90%, was used for the experiments. The characteristics of the tool are shown in Table 3, and its geometry is shown in Fig. 1.

3. Research Approach

3.1 Selection of Best Variables to Simulate an Orthogonal Machining Process Using DEFORM 2D Software

An orthogonal machining process was simulated using DEFORM 2D. To select the best variables to simulate an orthogonal cut, the resultant cutting forces obtained from the

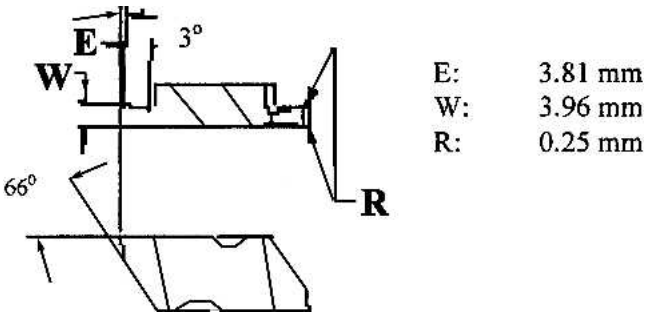

Fig. 1 Scheme of the tool used for the experiments

Table 4 Experimental cutting forces obtained under different cutting conditions (Ref 15)

Test	V, m/min	f(a), mm/rev	Fx_{exp}, N
1	121.9	0.127	348.4
2	121.9	0.178	452.4
3	182.9	0.127	327.8
4	182.9	0.152	382.8
5	182.9	0.178	412.4

(a) The feed rate is the depth of cut in an orthogonal cutting process.

Table 5 Boundary conditions used for the simulations

Boundary condition	Workpiece	Tool
Constraint displacement in X	BC	…
Constraint displacement in Y	AB-BC	FE-ED
Heat exchange with environment	AB-BC	FE-ED
Coefficient of friction at tool-chip interface	0.3	0.3
Tool movement	…	−X

simulations were validated by comparing them with previous experimental cutting force data (Table 4). For simplicity, the usual 2D plane strain condition was assumed. This is a reasonable assumption provided that the width of cut is significantly larger than the depth of cut. In view of significantly high elastic modulus of most tool materials, a perfectly rigid tool was modeled. This is also an acceptable approximation because the elastic deflection of the tool is secondary relative to the excessive plastic deformation of the work piece (Ref 8).

Because DEFORM 2D did not have the flow stress model for the material (AISI 52100) used in the experimental work (Ref 15), flow stress data for this steel was included (62 HRC). This flow stress data was obtained from previous research (Ref 16).

The following are the variables to be considered for the simulation of the orthogonal machining process using DEFORM 2D: workpiece geometry, numbers of elements in work piece, numbers of elements in tool, type of element use for the mesh of the workpiece and the tool, heat transfer coefficient at tool-chip interface, friction coefficient (sticky area), coulomb constant (sliding area), length of sticking region, time steps, and number of steps.

Table 5, shows the boundary conditions used for the simulations of an orthogonal cut and Fig. 2 shows the scheme of the general view of the FEM simulation using DEFORM 2D.

DEFORM 2D considers the Coulomb model as the friction model between the workpiece and the tool for the orthogonal

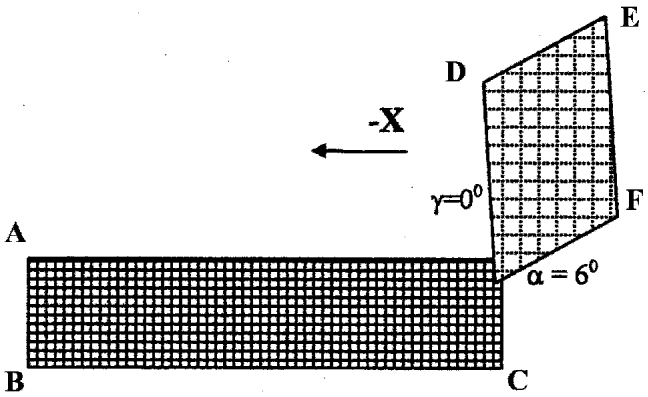

Fig. 2 Scheme of the general view of the FEM for simulation of an orthogonal cut using DEFORM 2D

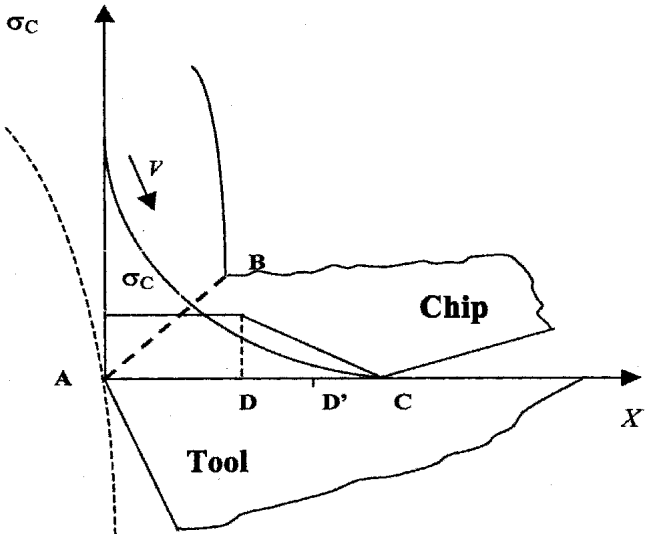

Fig. 3 Scheme of cut of the friction model considered for the orthogonal cutting process

cut simulation, considering a sliding and sticky area. Figure 3 shows the scheme of cut where these areas are located.

As observed in Fig. 3, line AC is the contact length between the tool rake angle (γ) and the chip. Also, it can be observed how the contact length AC is divided in two parts AD and DC. The shear stress (σ_c) is constant along AD but decreases to zero along DC, reaching the zero value when the chip stops touching the tool (point C). The sticky condition occurs in region AD and the sliding condition occurs in region DC.

3.2 Stress, Deformation, Rate Deformation and Temperature Generated during the Simulation Cutting Process

Once the best variables are known that simulate an orthogonal cutting process for AISI 52100 using DEFORM 2D (Sec. 3.1), simulations were done considering the feed rates (i.e., depth of cut in an orthogonal cut). This is shown in Table 6.

Values of cutting force, stress, deformation, deformation rate, and temperature for each cutting condition were selected for the work piece in the area located around the tool cutting

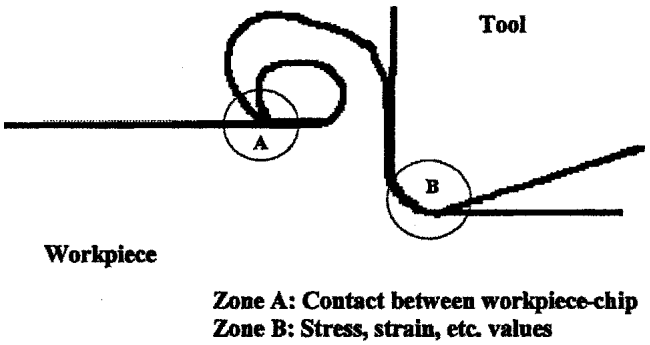

Fig. 4 Scheme of the moment when the chip touches the workpiece during the simulation of an orthogonal cut

Table 6 Selected cutting variables used for the experiments

Test	*f*, mm/rev
1	0.02
2	0.03
3	0.04
4	0.05
5	0.06
6	0.07

edge (zone B) and in the step before the chip touches the workpiece (zone A). This is shown in Fig. 4.

The experimental orthogonal cuts were carried out on a Hardinge super precision lathe (Model Conquest T 42 SP). The experimental cutting forces were measured with a dynamometer.

Samples, with $\varnothing_{ext} = 38.65$ mm, $\varnothing_{int} = 35.05$ mm and with a thickness of 2 mm, were obtained from each cutting condition according to the scheme shown in Fig. 5.

The experimental orthogonal cuts were done in the dry condition using a constant speed of $V = 120$ m/min. Each condition was done twice to assure reliable results. (See cutting conditions in Table 6). A tool with the same characteristics as shown in Table 3 and Fig. 1 was used for the experiments.

3.3 Surface Roughness Measurement

After the experimental orthogonal machining process was done for each cutting condition, the surface roughness was measured for all specimens in the four different areas (A, B, C, D), as shown in Fig. 6. Each area was measured five times along and across the feed cutting marks to obtain an average of the R_t, rms, and R_a surface roughness values. The surface roughness was measured using a white light interferometer with an objective of 10×, no filter, and a scan length of 20 μm bipolar (14 s).

4. Results and Discussion

4.1 Selection of Best Variables to Simulate an Orthogonal Machining Process Using DEFORM 2D

The simulations were done under the conditions shown in Tables 5 and 6. Once the experimental cutting forces were compared with the simulated cutting forces (considering the

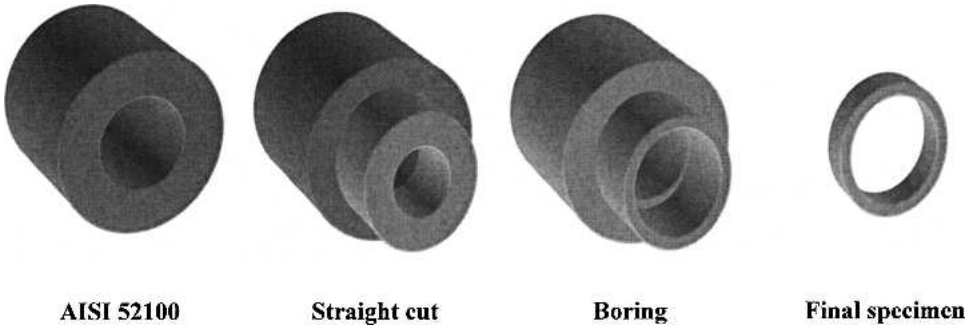

Fig. 5 Scheme of the sequence used for the experiments

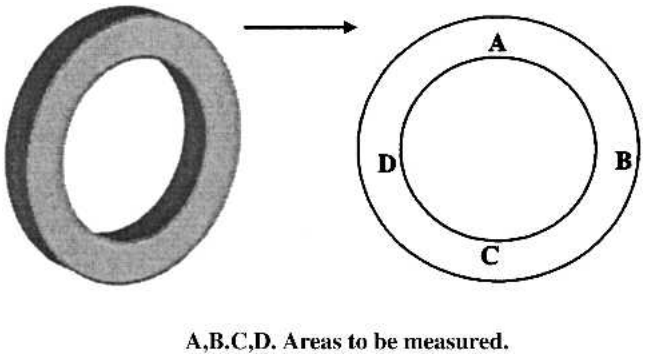

Fig. 6 Scheme of the resulted specimen obtained from the orthogonal machining process and the areas where the surface roughness was measured

Table 7 Variables for an orthogonal machining process simulation for AISI 52100 using DEFORM 2D

Workpiece material	Elastic-plastic
Workpiece geometry	3 × 1.127 mm
Number of elements in workpiece	5000
Tool material	Rigid
Tool geometry	0.587 × 1 mm: $\alpha = 5°$, $\gamma = 0°$, $R = 0.035$ mm
Numbers of elements in tool	1003
Type of element use for the mesh of the workpiece and the tool	4 nodes, Isoparametric plane strain elements
Heat transfer coefficient at tool-chip interface	11 W/m · K
Friction coefficient at sticky area	1
Coulomb constant at sliding area	0.3
Length of sticky region	Same as depth of cut
Time steps	1×10^{-7} s
Total number of step	4000

best variables for an orthogonal machining simulation) for the different trials with different variables, the following results (Tables 7 and 8) were obtained.

A difference of 20% between the experimental and simulated values was considered to be good (Ref 9). As can be observed, the simulated cutting forces obtained are very close to the experimental values (Table 7) and are the best values to simulate an orthogonal cut using DEFORM 2D under these experimental conditions.

Analyzing the results, the simulated cutting forces exhibit the same behavior as the experimental cutting forces. This is shown more clearly in Fig. 7.

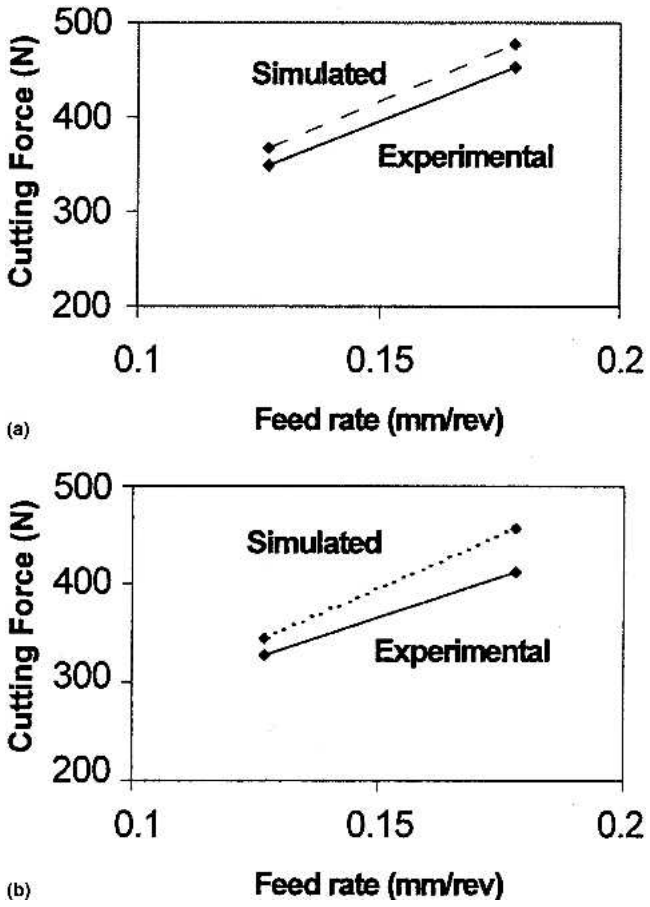

Fig. 7 Cutting force versus feed rate: (a) $V = 121.92$ m/min and (b) $V = 182.88$ m/min

Table 8 Experimental and simulated cutting forces (based on Table 4)

Test	Speed, m/min	Feed, mm/rev	Fx_{Exp}, N	Fx_{Simul}, N	Error, %
1	121.9	0.127	348.4	367.2	5.4
2	121.9	0.178	452.4	478.4	5.7
3	182.9	0.127	327.8	344.0	5.0
4	182.9	0.152	382.8	404.8	5.7
5	182.9	0.178	412.4	457.6	10.4

Figure 7 also shows an increase of almost 100 N in the cutting force upon increasing the feed rate 50% for a constant cutting speed. This behavior is due to the fact that the chips

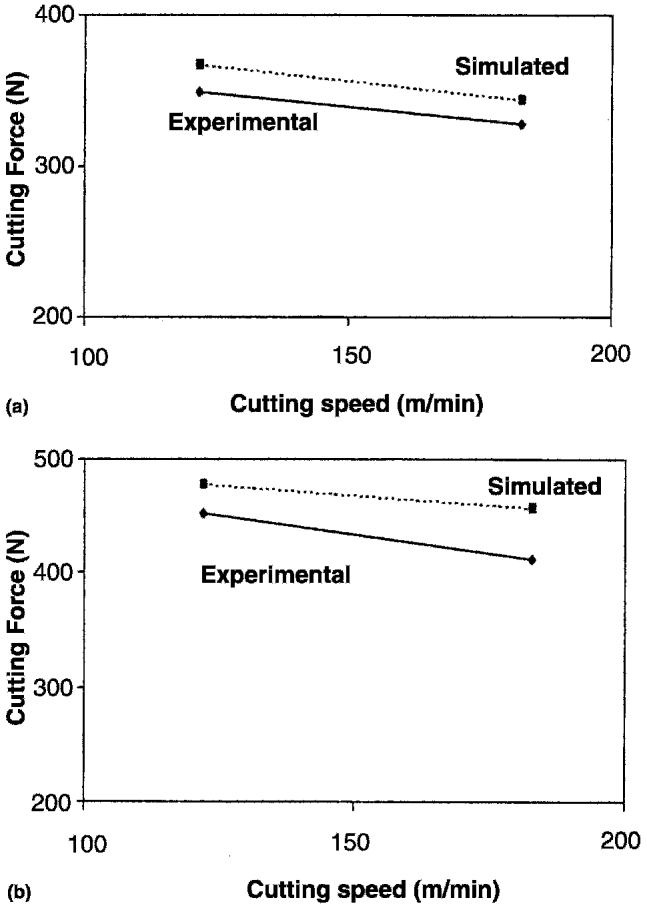

Fig. 8 Cutting force versus cutting speed: (a) $f = 0.127$ mm/rev and (b) $f = 0.178$ mm/rev

Table 9 Experimental, simulated, and error between cutting and thrust forces obtained as a result of the orthogonal machining process

Test	*f*, mm/rev	Fx_{exp}, N	Fx_{simul}, N	Fx, % error	Fy_{exp}, N	Fy_{simul}, N	Fy, % error
1	0.02	96.6	70.4	27.1	125.5	121.0	3.6
2		99.2		29.0	133.9		9.6
3	0.03	122.5	97.2	20.7	138.8	143.0	3.1
4		124.6		22.0	146.4		2.3
5	0.04	146.9	120.0	18.3	151.2	158.4	4.7
6		148.7		19.3	149.2		6.2
7	0.05	170.4	152.4	10.6	157.1	173.6	10.5
8		167.8		9.2	160.7		8.0
9	0.06	193.2	180.0	6.8	164.9	183.2	11.1
10		196.3		8.3	166.9		9.8
11	0.07	210.2	220.0	4.7	167.1	190.0	13.7
12		214.3		2.7	166.8		13.9

become larger as the feed is increased, producing higher compression of the tool against the working material, and leading to higher plastic deformation on the cutting area. This behavior is also in agreement with previous research (Ref 17-19).

When analyzing the influence of the cutting speed on the cutting force (Fig. 8), a slight decrease of around 30 N is observed for the cutting force when increasing the cutting speed 50% for a constant feed rate.

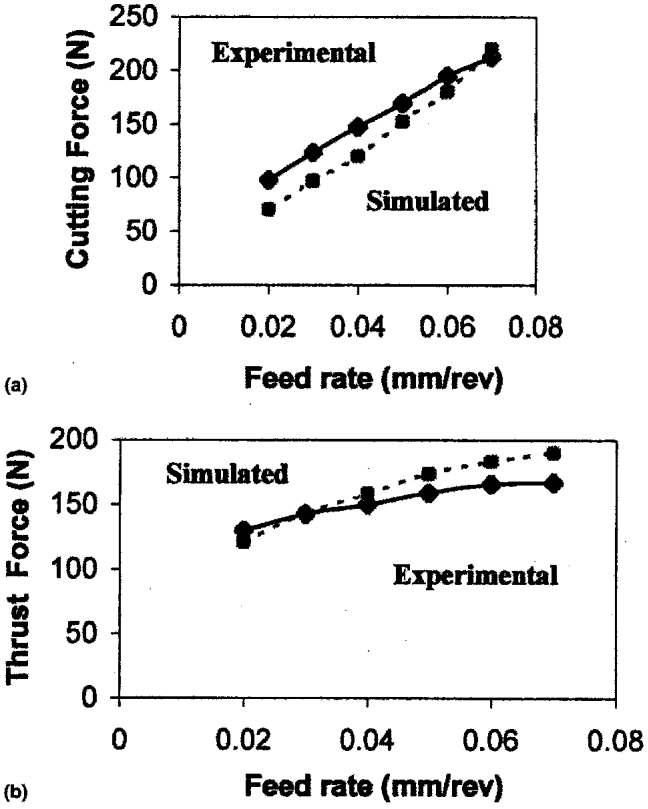

Fig. 9 (a) Cutting force versus feed rate and (b) thrust force versus feed rate for AISI 52100

Table 10 Results of simulated stress, strain, strain rate, and temperature in workpiece surface cut area after an orthogonal cut

f, mm/rev	Stress, MPa	Strain, mm/mm	Strain rate, mm/mm/rev	Temperature, °C
0.02	836.7	1.79	1.5 × 105	476.3
0.03	843.5	2.44	1.5 × 105	482.2
0.04	859.5	2.74	1.5 × 105	478.9
0.05	869.1	2.51	1.5 × 105	481.5
0.06	888.3	2.24	1.5 × 105	487.2
0.07	907.1	2.27	1.5 × 105	489.3

Previous research showed that the cutting speed does not have much influence on the cutting force compared with the other cutting variables such as feed rate, depth of cut and tool nose radius (Ref 19). These results agree with previous research when compared with cutting speed slopes (Fig. 8) and feed rate slopes (Fig. 7). Also, previous research showed that the cutting force is practically constant when the cutting speed is increased (Ref 4).

4.2 Simulated and Experimental Orthogonal Machining Process for AISI 52100 C Steel

Once the best values of the variables for simulating an orthogonal cut were selected (Table 7, Part 1), new simulations for AISI 52100 were done based on the results shown in Table 6. The experimental orthogonal cuts were carried out as before. The results obtained from this simulation and experiments are shown in Table 9.

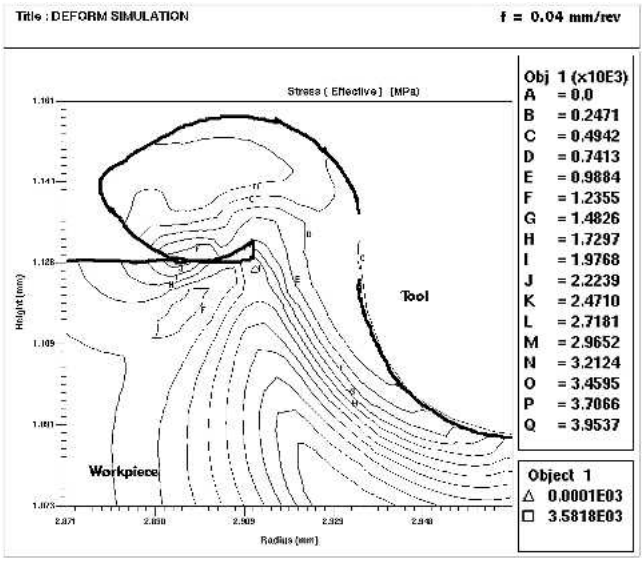

Fig. 10 Stress contour lines for $f = 0.04$ mm/rev

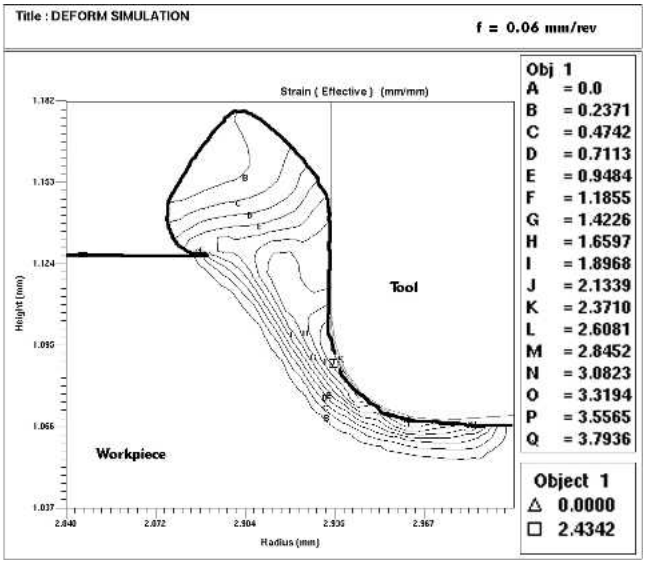

Fig. 12 Strain contour lines for $f = 0.06$ mm/rev

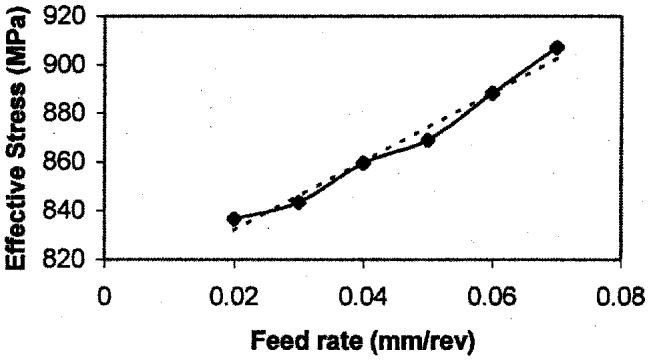

Fig. 11 Stress versus feed rate for AISI 52100 cut at $V = 120$ m/min

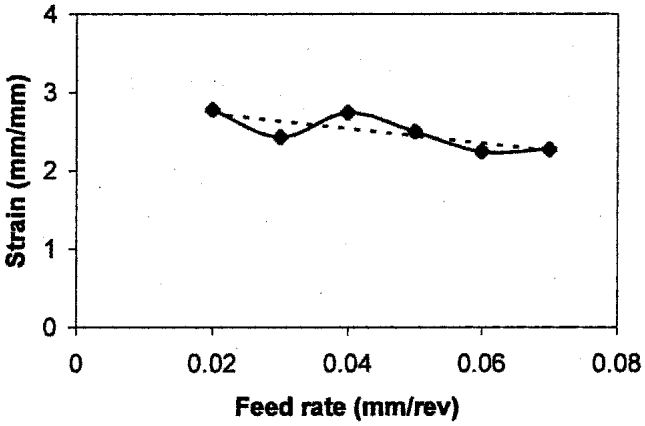

Fig. 13 Strain versus feed rate for AISI 52100 cut at $V = 120$ m/min

Because experimental cutting and thrust forces are very close to each other for each cutting condition, a third trial was not needed. As can be observed, the highest errors were obtained for $f = 0.02$ and 0.03 mm/rev. This is probably due to the fact that these feeds are lower than the tool cutting edge radius ($R = 0.035$ mm). Also, it was observed in general terms that the error between experimental and simulated cutting and thrust forces is less than 20%, making this a very good approach, and leading to very good results (Ref 9).

After each experimental run, the tools were observed in a microscope to evaluate the cutting edge radius and flank wear of the tool after each cut. Figure 9 shows the influence of the feed rate on the experimental and simulated cutting and thrust force. It can be observed that in both cases the force increases when the feed rate is increased. These results agree with previous research (Ref 17-19).

Table 10 shows the results of highest stress, strain, strain rate and temperature obtained in the workpiece surface cut area (Zone B, Fig. 4) after the simulation of an orthogonal machining process in the step were the chip starts to touch the workpiece.

Figures 10, 12, 14, and 16 show representative contour lines for stress, strain, strain rate and temperature for the step where

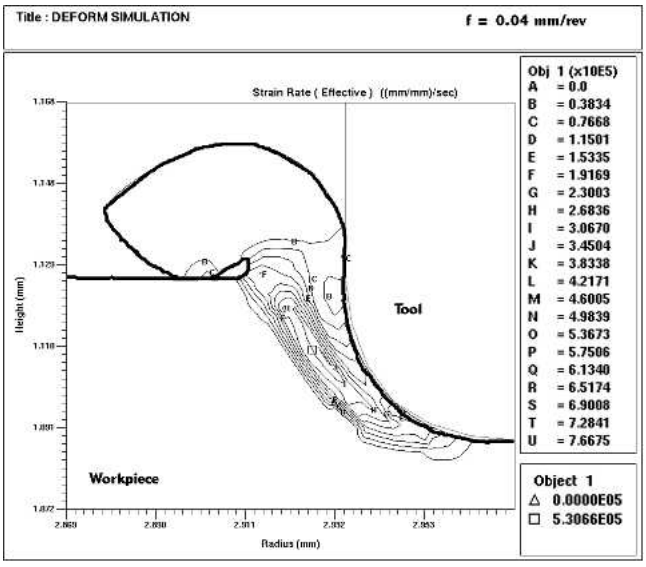

Fig. 14 Strain rate contour lines for $f = 0.04$ mm/rev

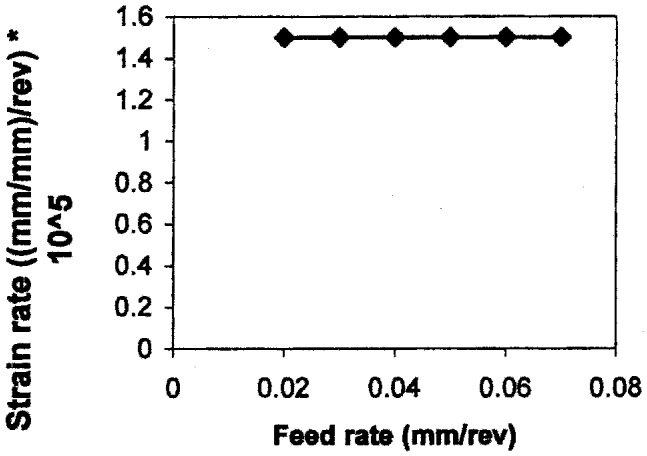

Fig. 15 Strain rate versus feed rate for AISI 52100 cut at $V = 120$ m/min

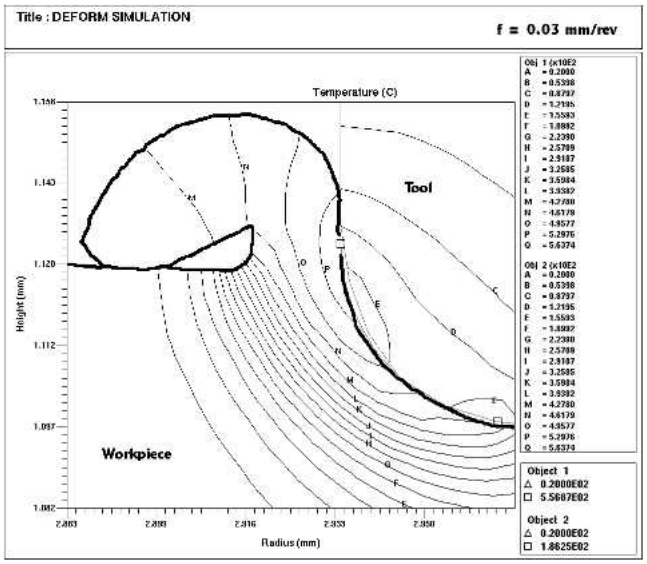

Fig. 16 Temperature contour lines for $f = 0.03$ mm/rev

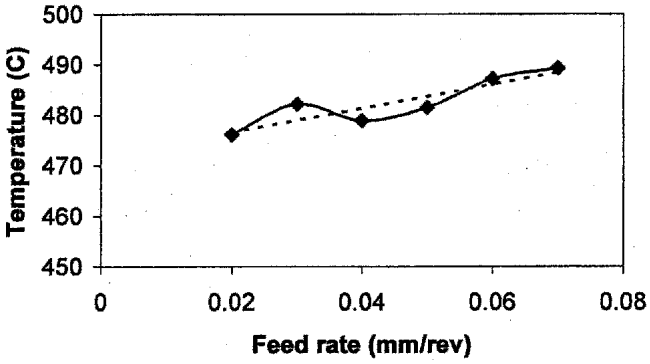

Fig. 17 Temperature versus feed rate for AISI 52100 cut at $V = 120$ m/min

Table 11 R_t, rms, and R_a from measurement across feed marks for each cutting condition

f, mm/rev	$R_t \pm 0.001$ μm	rms ± 0.001 μm	$R_a \pm 0.001$ μm
0.02	1.638	0.295	0.234
0.03	1.745	0.313	0.251
0.04	1.501	0.25	0.196
0.05	1.819	0.332	0.268
0.06	2.295	0.374	0.295
0.07	2.45	0.398	0.311

Table 12 R_t, rms, and R_a from measurement along feed marks for each cutting condition

f, mm/rev	$R_t \pm 0.001$ μm	rms ± 0.001 μm	$R_a \pm 0.001$ μm
0.02	1.111	0.308	0.155
0.03	1.059	0.195	0.209
0.04	0.969	0.185	0.145
0.05	0.904	0.163	0.127
0.06	1.457	0.274	0.215
0.07	1.440	0.275	0.214

the chip touches the workpiece (as shown in Fig. 4) for different cutting conditions.

From analysis of Fig. 10, it can be observed that, in general, higher values of stress occur in the primary deformation zone and a decrease in stress is observed in the secondary deformation zone. Due to the small rake angle used for the experiments ($\gamma = 0°$), very high stresses are imposed on the workpiece. Under these conditions, the workpiece shears along a plate, or thin zone (i.e., primary zone), where the stress is a maximum (Ref 20). Figure 11 shows more clearly the influence of the feed rate on the stress, where the tendency is increased stress when the feed is increased. Also, the experiments showed for all conditions that the chip size increases as the feed rate was increased.

From analysis of Fig. 12, it can be observed that in all cases higher values of strain were located in the primary deformation zone, and even though a define pattern was not observed, apparently the tendency is a decrease in this value when the feed rate is increased. This is probably due to the fact that as the feed is increased, the chip becomes larger. Since the contact area between the chip and the tool has increased, a uniform compression zone forms producing smoother deformation in this area. This behavior is also shown in Fig. 13, where strain is plotted against the strain of the workpiece surface cut area after the orthogonal machining simulation process.

From analysis of Fig. 14, it can be observed that the strain rate contour lines are located in the chip area and concentrated in the chip-rake face tool area. Also, it is shown that higher values of strain rates are in the chip tool interface zone. This result remains constant for all cutting conditions. Figure 15 shows the influence of the feed rate on the strain rate. In this figure, the strain rate remains constant as the feed rate is increased. This result is logical because for the simulations the strain rates were assume constant from 10^{-2} to 10^{6} mm/s since this steel has low strain rate sensitivity.

From analysis of Fig. 16, where temperature contour lines are shown for $f = 0.03$ mm/rev, it is seen that the temperature is higher in the contact zone between the chip and tool's rake face. This behavior was constant for all experimental conditions. This behavior results from the generation of heat during the cutting process due to the friction between the chip and tool. Figure 17 shows the influence of the feed rate on tem-

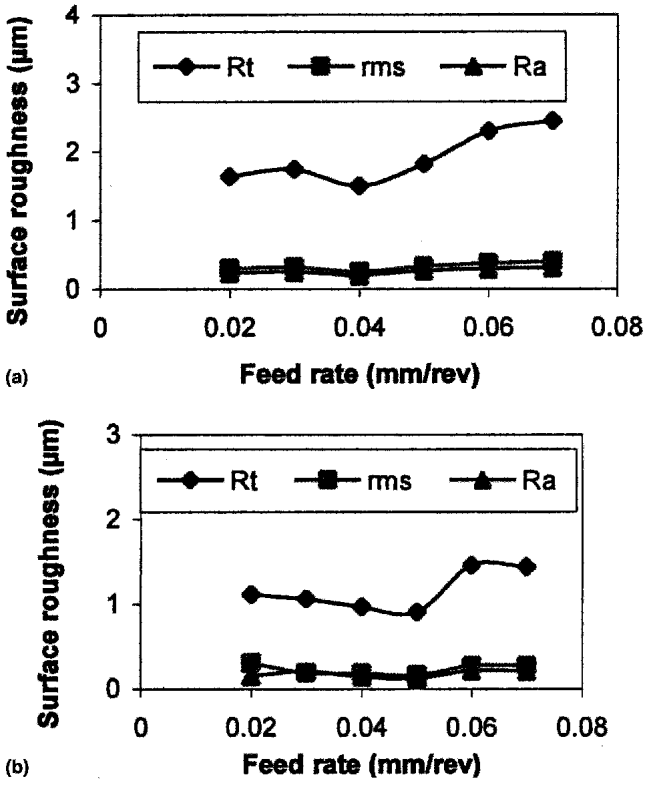

Fig. 18 Surface roughness versus feed rate, for AISI 52100: (a) across feed cut marks and (b) along feed cut marks

perature. In this figure, it is seen that the temperature increases as the feed rate is increased (i.e., depth of cut), since the contact area between chip and tool also increases due to an increase in the energy required for the cutting process.

4.3 Surface Measurement

As it was mentioned before, each specimen was measured five times along and across the feed marks in four different areas (A, B, C, and D). To obtain an average of the surface roughness value, extreme values were ignored on each test. Tables 11 and 12, shows the total average of the R_t (maximum roughness height), rms (root-mean-square average), and R_a (arithmetic mean value), across and along the feed cut marks. Figure 18 shows the influence of the feed rate on the R_t, rms, and R_a values across and along the feed cut marks.

Figure 18 shows that feed rate has more influence on R_t than rms and R_a. Also, the surface roughness decreases between 0.02 and 0.04 mm/rev and increases from this last value of feed rate. This behavior is more noticeable on an R_t plot, and a very slight effect can be observed on rms and R_a plots. This behavior is probably due to the fact that the tool edge radius is smaller than 0.04 mm.

Because these results showed that the feed rate has more influence on the R_t values of surface roughness, this variable was plotted against the values of stress, strain and temperature. Figures 19-21 show the influence of stress, temperature and strain obtained in the workpiece surface cut area due to the orthogonal machining process simulation on the surface

From Fig. 19-21, the behavior of R_t across and along the feed cut marks is the same. In Fig. 19 and 20, the R_t values, in general, increase when the stress and the temperature are increased.

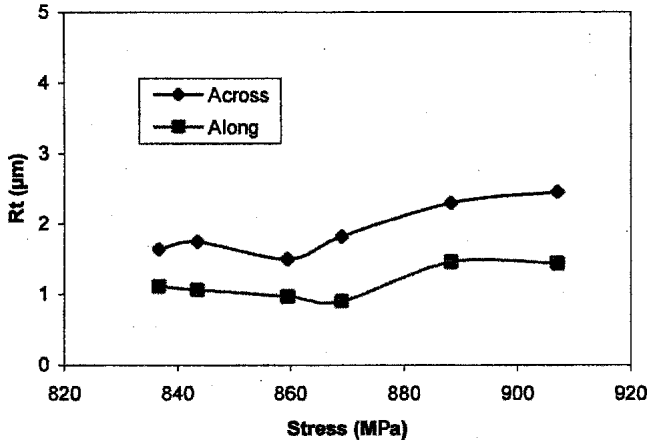

Fig. 19 R_t versus stress for AISI 52100

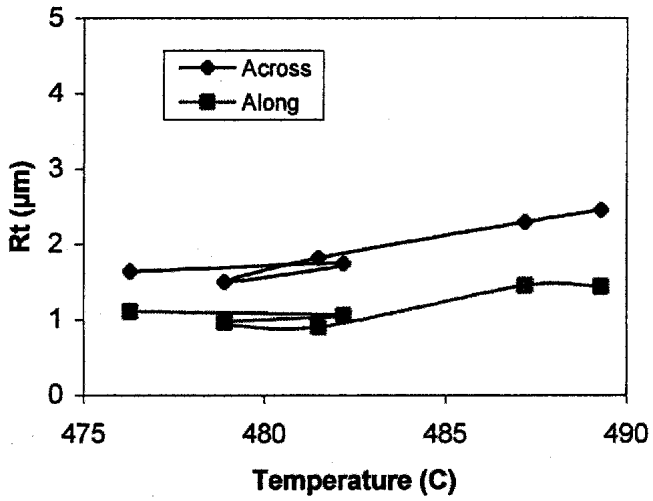

Fig. 20 R_t versus temperature for AISI 52100

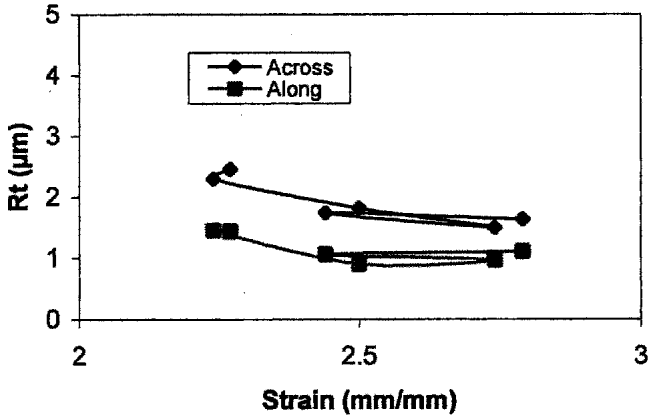

Fig. 21 R_t versus strain for AISI 52100

This result is due to the fact that these values (i.e., stress and temperature) increase when the feed rate is increased (Fig. 11 and 17). Because the feed is higher, the chip becomes larger producing an increase of the contact area between the chip and the tool, and giving rise to an increment of friction. In addition, this is a rough way to remove material from the workpiece surface.

In Fig. 21, where the influence of the strain on R_t is plotted, it was observed that surface roughness improves slightly when the strain increases. This result is probably due to the uniform contact between the chip and the tool as the feed rate is increased.

5. Conclusions

- It was verified that the cutting and thrust forces increase when the feed rate is increased.
- It was verified that the cutting forces are almost constant when the cutting speed is increased.
- Higher values of stress are located in the primary deformation zone.
- Higher values of strain and temperature are located in the secondary deformation zone.
- Stress and temperature increase when the feed rate is increased.
- Strain decreases when the feed rate is increased
- Feed rate has more influence on the R_t than on rms and R_a.
- Surface roughness increases when the feed rate is increased, and this is more noticeable for R_t.
- Surface roughness (R_t) increases with an increase of stress and temperature and decreases with a decrease of the strain.

References

1. M.E. Merchant, Mechanics of the Metal Cutting Process, *J. Appl. Physics,* Vol 16 (No. 6), 1945, p 318-324
2. E.H. Lee and B.W. Schaffer, Theory of Plasticity Applied problems of Machining, *ASME J. Appl. Mech.,* Vol 18 (No. 4), 1951, p 104-113
3. A.O. Tay, M.G. Stevenson, and G. De Vahl Davis, Using the Finite Element Method to Determine Temperature Distributions in Orthogonal Machining, *Proc Inst. Mech. Eng.,* Vol 188, 1974, p 627-637
4. W.F. Hasting, P. Mathew, and P.L.B. Oxley, A Machning Theory for Predicting Chip Geometry, Cutting Forces, Etc., From Work Material Properties and Cutting Conditions, *Proc. Royal Soc. (London),* Vol A 371, 1980, p 569-587
5. D. Lee, The Nature of Chip Formation in Orthogonal Machining, *J. Eng. Mater. Technol.,* Vol 106, 1984, p 9-15
6. J.S. Strenkowski and J.T. Carrol, A Finite Element Model of Orthogonal Metal Cutting, *J. Eng. Industry,* Vol 107, 1985, p 349-354
7. T.H.C. Childs and K. Maekawa, Computer-Aided Simulation and Experimental Studies of Chip Flow and Tool Wear in the Turning of Low Alloy Steels by Cemented Carbide Tools, *Wear,* Vol 139, 1990, p 235-250
8. K. Komvopoulos and S.A. Erpenbeck, Finite Element Modeling of Orthogonal Metal Cutting, *J. Eng. Industry,* Vol 113, 1991, p 253-267
9. B. Zhang and A. Bagchi, Finite Element Simulation of Chip Formation and Comparison with Machining Experiment, Computational Methods in Materials Processing, PED-Vol. 61, ASME, 1992, p 61-74
10. G.S. Sekhon and J.L. Chenot, Numerical Simulation of Continuous Chip Formation During Non-Steady Orthogonal Cutting, *Eng. Comp.,* Vol 10, 1993, p 31-48
11. E.G. Ng, D.K. Aspinwall, D. Brazil, and J. Monagham, Modelling of Temperature and Forces when Orthogonally Machining Hardened Steel, *Int. J. Mach. Tools Manuf.,* Vol 39, 1999, p 885-903
12. S. Chandrakanth and X. Deng. Finite Element Analysis of the Orthogonal Metal Cutting Process, *J. Mater. Proc. Technol.,* Vol 105, 2000, p 95-109
13. A.G. Mamalis, M. Horvath, A.S. Branis, and D.E. Manolakos, Finite Element Simulation of chip Formation in Orthogonal Metal Cutting, *J. Mater. Proc. Technol.,* Vol 110, 2001, p 19-27
14. M.H. Dirikolu, T.H.C. Childs, and K. Maekawa, Finite Element Simulation of Chip Flow in Metal Machining, *Inter. J. Mech. Sci.,* Vol 43, 2001, p 2699-2713
15. A. Ramesh, "Prediction of Process-Induced Microstructural changes and Residual Stresses in Orthogonal Hard Machining," Ph.D. Dissertation, Georgia Institute of Technology, Atlanta, GA, June 2002
16. G. Toledo, "High Temperature Compression Testing of Hardened Steels for Plasticity Behavior Modeling," MS Thesis, Georgia Institute of Technology, Atlanta, GA, 2002
17. H.T.Young and P. Mathew, Allowing for Nose Radius Effects in Predicting the Chip Flow and Cutting Forces in Bar Turning, *Proc. Inst. Mech. Eng.,* Vol 201 (No. C3), 1987, p 213-226
18. Y.S. Tarng and T.S. Hwang, An Investigation of the Specific Cutting Force and its Direction Factors in Turning, *Comp. Struct.,* Vol 53 (No. 4), 1994, p 937-945
19. Z. Cassier, P. Munoz-Escalona, and R. Sanchez, Influence of the Cutting Parameters on the Cutting Forces of Carbon Steel, *ASME,* 2002, p 117-121
20. J. Datsko, *Materials Selection for Design and Manufacturing: Theory and Practice,* Marcel Dekker, Inc., New York, 1997, p 177-280 and 307-324